Micelles Formed by an AB Copolymer with Bottlebrush Blocks: Scaling Theory

Ekaterina Zhulina, Oleg Borisov

Micelles Formed by AB Copolymer with Bottlebrush Blocks. Scaling Theory.

Ekaterina B.Zhulina[1], Oleg V. Borisov[1,2*]
[1]Institute of Macromolecular Compounds
of the Russian Academy of Sciences,
199004 St.Petersburg, Russia
[2]Institut des Sciences Analytiques et de Physico-Chimie pour
l'Environnement et les Matériaux, UMR 5254 CNRS UPPA,
64053 Pau, France

October 5, 2021

Abstract

We present a scaling theory describing equilibrium properties of spherical micelles formed by diblock copolymer with bottlebrush blocks in selective solvent. The theory predicts a number of new thermodynamic regimes inherent for copolymers with relatively short main chains (long side chains) in the bottlebrush blocks. These regimes with a novel set of scaling exponents for the micelle properties are characterized by limiting extension of the main chains of the core or/and corona-forming blocks and do not exist for micelles of conventional linear block copolymers. The theoretical predictions are confronted to experiments.

email: oleg.borisov@uiv-pau.fr

TOC Graphic

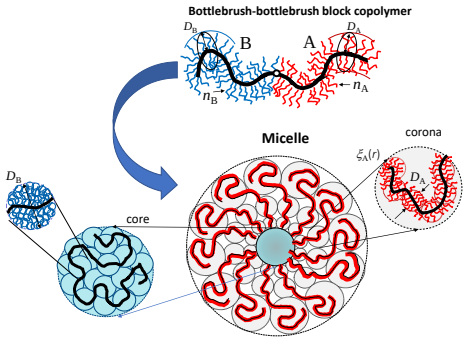
Bottlebrush-bottlebrush block copolymer
B
A
Micelle
corona
core

1 Introduction

Self-assembly of block copolymers with various architectures of the blocks remains in the focus of research for a number of decades. Interest to these systems is dictated by potential and emerging applications in nanomedicine as drug carriers,[1] biomimetic design,[2] tissue-engineering,[3] etc. Self-assembling spherical micelles formed by AB and ABA block copolymers have been extensively studied experimentally (see, e.g., reviews[4–6]) and theoretically (see, e.g., review[7]).

Scaling concepts[8] and theories of polymer solutions and brushes[9,10] provided a foundation to specify the structure of polymer micelles in various solvents and solution concentrations. Depending on relative dimensions of the core and corona, spherical micelles were classified as crew-cut (with the corona thickness smaller than the core size) and starlike (with the corona thickness larger than the core size). The original model of crew-cut micelles introduced by de Gennes[11] paved the way to the scaling theories of starlike micelles.[12–14] The latter utilized blob concepts to envision the corona of starlike micelle as densely packed system of the concentration blobs with size increasing to the periphery of corona, and the core densely packed with the thermal blobs. Because soluble corona prevent precipitation of block copolymer in sediment, micelles could remain thermodynamically stable in a wide range of solution concentrations by adjusting their size, shape, and packing.[15–17] The scaling models provided asymptotic power law dependences for micelle equilibrium parameters (aggregation number, core and corona sizes, cmc) as a function of molecular weights of the blocks and solvent selectivity, and served as guidelines to rationalize the experimental data.[18]

Similarly to associating polymers,[19] micelles of ABA block copolymers form physical networks in solutions that makes them self-assembling precursors for gels with predictable and tunable properties. The advances in synthetic chemistry allowed for bottlebrush (bb) branching of the blocks that mediates mechanical properties of the forming gels and elastomers.[?] The latter depend on the architecture of the blocks that governs the equilibrium structure of micelles. Since power law dependences for the equilibrium parameters of ABA micelles are not changed by bridging *via* corona blocks, understanding the behavior of micelles formed by AB block copolymers with branched blocks could provide guidelines to manipulate the properties of ABA gels with bottlebrush strands.

The goal of this paper is to develop a scaling theory of polymer micelles formed by AB diblock copolymers with bottlebrush (bb) blocks. In our previous study[20] we considered such assemblies in the framework of the analytical self-consistent field (SS-SCF) theory with focus on the effect of architecture of

corona blocks on the equilibrium micelle parameters. The scf model allowed us to consider block copolymers with starlike (short backbone) and bottlebrush (long backbone) blocks in a unified way, and to examine crossovers between different regimes. It was demonstrated that self-assemblies with branched corona blocks exhibit a more diverse behavior compared to micelles formed by AB diblock copolymers with linear blocks.[12,13] In particular, different elastic responses of starlike and bottlebrush blocks to elongation led to separate regimes in the diagram of states for micelles with branched corona. At the same time local structure of the side chains in the vicinity of backbones was out of scope of the scf model.

In this paper we implement scaling concepts to diblock copolymers that comprise long backbones in both bb blocks, and construct the scaling-type diagram of states for block copolymer assemblies in a dilute solution. These findings illuminate the effect of local structure of bb blocks and serve as foundation to consider micelle rearrangements in semi-dilute solutions. The rest of the paper is organized as follows. In section II we describe the model of a spherical micelle with bb branched blocks and introduce the concept of superblob. In sections III and IV we consider dilute solutions of starlike and crew-cut micelles while in section V discuss the theoretical predictions, confront them to experiments, and formulate the conclusions.

2 Model

We consider diblock copolymers comprising two chemically different bottlebrush blocks, **Figure 1a**. Block A has total degree of polymerization (DP) N_A, DP of backbone M_A, and DPs n_A and m_A of the side chains and spacer separating neighboring grafting points. The ratio $1/m_A$ (number of side chains per monomer unit of the main chain) quantifies grafting density. Below we assume $n_A/m_A \gg 1$ (the bottlebrush regime). Total number of side chains in the block A is M_A/m_A. Block B with total DP N_B is characterized by the corresponding set of parameters: M_B, n_B and m_B. Evidently, $n_i = 0$ with $i = A, B$ correspond to the respective linear blocks. The DPs of the blocks are expressed as

$$N_i = M_i(1 + \frac{n_i}{m_i}) \qquad\qquad i = A, B \tag{1}$$

The backbone and the side chains in both blocks are assumed to be intrinsically flexible, that is, the monomer unit size a (the same for both blocks), is on the order of the Kuhn segment length. Below we focus on densely grafted bottlebrush blocks with $m_i \simeq 1, i = A, B$ that are directly relevant

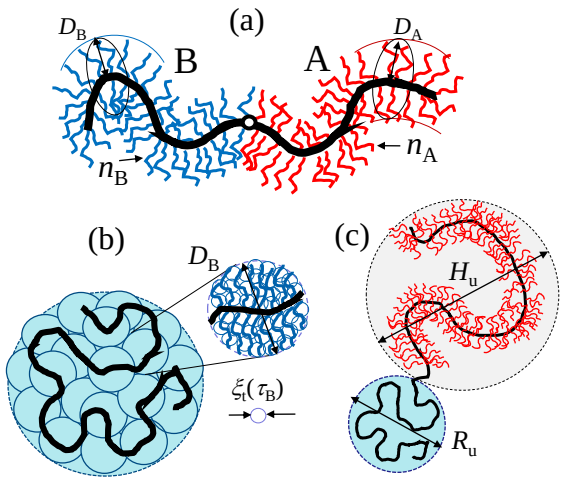

Figure 1: Schematics of AB diblock copolymer with bottlebrush blocks, $m_A = m_B \cong 1$. Backbones in both blocks are indicated by thick black lines. n_A and n_B are the DPs of the side chains in A and B blocks, respectively. D_A and D_B are crossectional thicknesses of respective bottlebrush blocks (a). Individual condensed block B (a globule) envisioned as a close packed array of superblobs of size D_B; the size of thermal blob is $\xi_t \cong a/\tau_B$, (b). AB bb block copolymer in the unimer state; H_u and R_u are the resepctive dimensions of swollen block A and collapsed bolck B (c).

to many experiments.[21–28] The solvent is assumed to be poor for block B and vary from athermal to theta-solvent for block A. The latter is envisioned as wormlike chain with thickness D_A and the effective Kuhn length L_A. In melts, $D_A \simeq a n_A^{1/2}$ and $L_A \simeq D_A$, in agreement with MD simulations[29] The flexibility of bottlebrushes in solution remained a subject of discussions in the literature for a long time.[30–40] In this paper we implement $L_A \simeq D_A$ as suggested originally in ref.[30] and confirmed by scf simulations[37] for bb polymers with DP of side chains $n_A \lesssim 100$. On length scales smaller than D_A, side chains form a cylindrical brush around strongly stretched backbone, while on length scales larger than D_A, bb block A exhibits the excluded volume behavior, similar to that of a linear chain of monomer units with size D_A in a good solvent.

In the framework of scaling model,[12,13] a cylindrical brush of side chains with DP n and $m \simeq 1$ is envisioned as a system of densely packed concentration blobs with size $\xi(\rho) \simeq \rho^{1/2}$, and volume fraction profile $c(\rho)$ of monomer units,

$$c(\rho) \simeq \tau^{(1-2\nu)/\nu} \left(\frac{a}{\rho}\right)^{(3\nu-1)/2\nu} \tag{2}$$

Here ρ is the distance from the backbone, the solvent quality is specified by absolute value of the relative deviation from θ-point, $\tau = \mid T - \theta \mid /T \geq 0$, with $\nu = 3/5$, $1/2$, or $1/3$ under good, theta, and poor solvent conditions, respectively.

Normalization condition

$$\int_a^D c(\rho)\rho d\rho = a^2 n$$

provides thickness D of the cylindrical brush,

$$D \simeq a\tau^{2(2\nu-1)/(\nu+1)} n^{2\nu/(\nu+1)} \tag{3}$$

2.1 Size of superblob D_A

For soluble block A, exponent ν in eq 2 is equal to 3/5 (good solvent conditions) or 1/2 (theta-solvent conditions). By substituting $\tau = \tau_A$ and $n = n_A$ in eq 3, one finds thickness D_A of bb block A,

$$D_A \simeq a\tau_A^{2(2\nu-1)/(\nu+1)} n_A^{2\nu/(\nu+1)} \tag{4}$$

The backbone segment in each superblob comprises D_A/a monomer units, and in both cases D_A is larger than unperturbed size of the side chain,

$D_A \geq \tau_A^{(2\nu-1)} n_A^{\nu}$, due to the elastic stretching invoked by repulsive binary (good solvent) or ternary (theta-solvent) monomer-monomer interactions. The asymptotic expressions for D_A in eq 4 are attained at $n_A \gg 1$ while computer simulations of bottlebrushes with moderately long side chains point at smaller values of apparent exponents.[41]

In the scaling model,[42] cylindrical layers in the brush of side chains are filled with concentration blobs with size $\xi_A(\rho) \simeq \rho^{1/2}$. The chain segments in the inner part of the brush with concentration $c_A(\rho) \geq \tau_A$ are found under theta-solvent conditions, while segments in the outer part of the brush with $c_A(\rho) \leq \tau_A$ are found under good solvent conditions. The boundary ρ^* between these two parts of the brush is specified as $\rho^* \simeq a\tau_A^{-2}$. The whole brush is found under theta-solvent conditions if $D_A(\nu = 1/2) \leq \rho^*$, or, equivalently, $\tau_A \leq n_A^{-1/3}$. In the opposite case of $\tau_A \geq n_A^{-1/3}$, the outer part of cylindrical brush with thickness $D_A - \rho^* \gg \rho^*$ is under good solvent conditions, while the sublayer with thickness $\rho^* \simeq a\tau_A^{-2}$ around the backbone remains under theta-solvent conditions. In the latter case the thickness of bb block A is dominated by the outer part of the brush with $D_A \approx D_A(\nu = 3/5)$.

Soluble block A gives rise to

$$N_{AS} = \frac{aM_A}{D_A} \tag{5}$$

of superblobs (effective monomers with size D_A) that are essentially impermeable due to the elastic stretching of side chains normally to the backbone. In the case of short (oligomeric) side chains with $n_A \simeq 1$, and $D_A \simeq a$, bb block A is treated as linear with DP M_A.

2.2 Size of superblob D_B and collapse of block B

A cylindrical brush of side chains with DP n_B and thickness D_B gives rise to

$$N_{BS} = \frac{aM_B}{D_B} \tag{6}$$

superblobs in block B. Under theta-solvent conditions, $D_B \simeq an_B^{2/3}$ ($\nu = 1/2$ in eq 3 with $n = n_B$), and the size of peripheral concentration blob $\xi_B(D_B) \simeq D_B^{1/2} \simeq n_B^{1/3}$. The threshold of brush condensation[42] is specified by equality of the peripheral concentration blob with size $\xi_B(D_B) \simeq D_B^{1/2}$ to the thermal blob with size $\xi_t \simeq a/\tau_B$, where $\tau_B = (\theta_B - T)/T$ to give the condensation threshold $\tau_B^* \simeq n_B^{-1/3}$. Notably, dense grafting of the side chains with $m_B \simeq 1$ shifts onset of the brush condensation to the values of τ_B larger than for homologous linear chains with DP n_B, $\tau_B^{*lin} \simeq n_B^{-1/2}$.

At $\tau_B > n_B^{-1/3}$, the inner part of the brush with thickness $\rho^* \simeq a/\tau_B^2$ remains unperturbed, i.e., retains the same structure as under theta-solvent conditions, while the outer part with thickness $(D_B - \rho^*)$ is densely packed with the thermal blobs. Because major fraction of monomer units is located in the outer (condensed) part of the superblob, its thickness D_B can be found by substituing $\nu = 1/3$ and $\tau = \tau_B$ in eq 3,

$$D_B \approx a \left(\frac{n_B}{\tau_B}\right)^{1/2} \tag{7}$$

While D_B decreases upon increasing τ_B, side chains remain stretched with respect to the Gaussian size, $D_B > a n_B^{1/2}$, and the brush retains its longitudinal stability[43] up to $\tau_B \simeq 1$.

The surface energy losses at the superblob-solvent interface invoke the attractive interactions between superblobs. As demonstrated in **SI**, in the vicinity of $\tau_B \simeq n_B^{-1/3}$ the second virial coefficient υ_D of superblob-superblob interactions changes from $\simeq D_B^3$ to $\simeq -D_B^3$, and the volume fraction c_D of superblobs in the condensed state yields

$$c_D = \frac{aN_B}{n_B D_B} \simeq -\frac{\upsilon_D}{D_B^3} \simeq 1$$

indicating dense packing of superblobs with intraglobular volume fraction of monomer units $c_B \simeq \tau_B$. Comparison of the average dimensions, R_u, of individual (unimer) block B under theta-solvent conditions (i.e., $R_u \simeq D_B(aM_B/D_B)^{3/5} \simeq aN_B^{3/5} n_B^{-1/3}$ at $\tau_B \leq n_B^{-1/3}$) and in poor solvent (i.e., $R_u \simeq a(N_B/\tau_B)^{1/3}$ at $\tau_B \geq n_B^{-1/3}$) indicates sharp coil-to-globule transition at $\tau_B \simeq n_B^{-1/3}$. Recall that in the framework of scaling model, bb block B in theta-solvent exhibits the excluded volume behavior ($R_u \sim N_B^{3/5}$) due to the stretched side chains, and, in contrast to the second virial coefficient in linear polymers, υ_D changes abruptly upon inferior solvent strength. Below we assume $\tau_B > n_B^{-1/3}$ to ensure the condensed state of block B with $c_B \simeq \tau_B$, see **Figure 1b**.

2.3 AB unimer

In a selective solvent, insoluble block B condenses in a globule with radius $R_u \simeq a(N_B/\tau_B)^{1/3}$ while block A ensures the solubility of block copolymer in the solution. The average size H_u of a single block A is governed by repulsive superblob-superblob interactions, and exhibits the excluded volume statistics on length scales larger than D_A. That is,

$$H_u \simeq D_A N_{AS}^{3/5} \simeq a^{3/5} D_A^{2/5} M_A^{3/5} \tag{8}$$

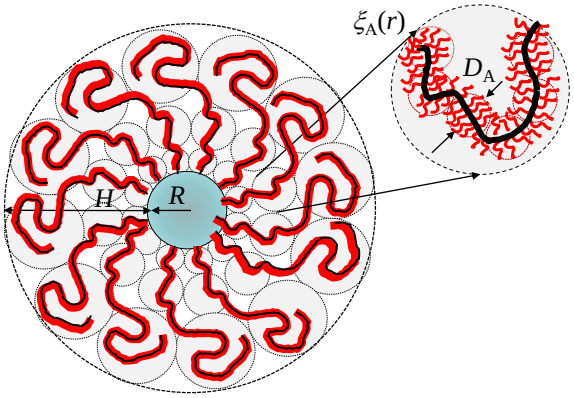

Figure 2: Blob structure of starlike micelle (regime ST in diagram of states). Increasing in size concentration blobs $\xi_A(r)$ are indicated in light grey.

with the solvent quality for the A-block manifested *via* $D_A(\tau_A)$ dependence, eq 4. In all the regimes of starlike micelles considered below, $R_g \ll H_u$, as illustrated in **Figure 1c**.

If, however, block A is linear with DP N_A, then H_u is governed by the solvent quality directly as

$$H_u \simeq a\tau_A^{(2\nu-1)} N_A^{\nu} \tag{9}$$

In the following we asign $\tau_A = 1$, and consider the cases of athermal ($\nu = 3/5$) and theta ($\nu = 1/2$) solvents for block A.

3 Starlike micelles

Poor solubility of blocks B drives association of block copolymers that leads to self-assemblies (micelles) in which blocks B constitute core domain with volume fraction $c_B \sim \tau_B$ of monomer units whereas soluble blocks A protrude into solution in the form of corona. The equilibrium aggregation number Q in a spherical micelle with flexible core and corona blocks can be found by

optimizing the free energy F per molecule that comprises the free energies F_A and F_B of blocks A and B, and the surface free energy $F_{A/B}$ at the core/corona interface,

$$F = F_A + F_B + F_{A/B} \tag{10}$$

We first consider starlike micelles in which corona thickness H exceeds by far radius R of the spherical core, $H > R$, see **Figure 2**. In a dilute solution, corona of starlike micelle is envisioned as a system of densely packed concentration blobs with size $\xi_A(r) \simeq r/Q^{1/2}$ where r is the distance from the center of micellar core. Inside concentration blob with size $\xi_A(r)$, the chain segment with number g_A of superblobs exhibits the excluded volume statistics, and g_A is specified as

$$\xi_A(r) \simeq \frac{r}{Q^{1/2}} \simeq D_A g_A^{3/5} \tag{11}$$

to give $g_A \simeq \xi_A^{5/3}(r)/D_A^{5/3}$. The average volume fraction $c_A(r)$ of monomer units at distance r from the core center yields

$$c_A(r) \simeq \frac{a^3 g_A}{\xi_A^3(r)} \left(\frac{D_A}{a} n_A\right) \simeq \left(\frac{\xi_A(r)}{a}\right)^{-4/3} \left(\frac{a}{D_A}\right)^{2/3} n_A \simeq Q^{2/3} \left(\frac{a}{r}\right)^{4/3} \left(\frac{a}{D_A}\right)^{2/3} n_A \tag{12}$$

Based on the blob concepts, the free energy F_A per block A can be evaluated as the total number of concentration blobs (with $\simeq k_B T$ per blob),

$$\frac{F_A}{k_B T} \simeq \int_R^{R+H} \frac{r^2}{Q} \xi_A^{-3} dr \simeq \int_R^{R+H} \frac{r^2}{Q} \frac{Q^{3/2}}{r^3} dr = Q^{1/2} \ln(1 + \frac{H}{R}) \approx Q^{1/2} \ln(\frac{H}{R}) \tag{13}$$

It should be emphasized that the total free energy of bb block A includes the "internal" contribution $\sim M_A D_A^{1/2}$ due to the elastic and interaction free energies of the side chains inside superblobs, and the free energy contribution accounting for superblob-superblob interactions (F_A in eq 13). Although the "internal" contribution is much larger, it does not depend on aggregation number Q and is omitted from consideration.

The core of micelle is envisioned as densely packed system of the thermal blobs with size $\xi_t \simeq a c_B^{-1} \simeq a/\tau_B$. The interaction free energy of the side chains ($\simeq -k_B T N_B \tau_B^2$ per block B) does not depend on aggregation number Q, and is omitted from consideration. The elastic free energy F_B of block B envisioned as linear chain of N_{BS} superblobs with size D_B yields

$$\frac{F_B}{k_B T} \simeq \frac{R^2}{D_B^2 N_{BS}} \simeq \left(\frac{Q N_B}{\tau_B}\right)^{2/3} \frac{n_B^{1/2} \tau_B^{1/2}}{N_B} \simeq Q^{2/3} N_B^{-1/3} n_B^{1/2} \tau_B^{-1/6} \tag{14}$$

The surface free energy $F_{A/B}$ per molecule is evaluated as the number of concentration blobs B per surface area $s \simeq R^2/Q$,

$$\frac{F_{A/B}}{k_BT} \simeq \frac{R^2}{Q\xi_B^2} \simeq \left(\frac{QN_B}{\tau_B}\right)^{2/3} \frac{(\tau_B)^2}{Q} \simeq \frac{{\tau_B}^{4/3}N_B^{2/3}}{Q^{1/3}} \tag{15}$$

If $F_B \ll F_A$, or, equivalently, $Q \ll N_B^2\tau_B n_B^{-3}$, minimization of F with respect to Q reduces to balance $F_A \simeq F_{A/B}$, to provide the power law dependence for aggregation number,

$$Q \simeq \frac{{\tau_B}^{8/5}N_B^{4/5}}{\ln^{6/5}(H/R)} \tag{16}$$

The thickness $H$of corona is specified as for a starlike polymer with monomer size D_A and DP N_{SA} in athermal solvent,[44]

$$H \simeq D_A N_{SA}^{3/5} Q^{1/5} \simeq a M_A^{3/5} \left(\frac{D_A}{a}\right)^{2/5} Q^{1/5} = a M_A^{3/5} (D_A/a)^{2/5} ({\tau_B}^2 N_B)^{4/25} \tag{17}$$

Similarly to aggregation number Q, the core radius

$$R \simeq (QN_B/\tau_B)^{1/3} \simeq a\tau_B^{1/5} N_B^{3/5} \left(\ln \frac{H}{R}\right)^{-2/5} \tag{18}$$

and interface area

$$s \simeq \frac{R^2}{Q} \simeq a^2 \tau_B^{-6/5} N_B^{2/5} \tag{19}$$

are weakly affected by bb branching of both blocks (*via* logarithmic prefactors in eqs 18,16).

As it follows from eqs 18 and 17, micelles remain starlike with $H \geq R$ if

$$M_A > \frac{N_B^{11/15}}{\tau_B^{1/5}} \left(\frac{a}{D_A}\right)^{2/3} \simeq M_B^{11/15} \tau_B^{8/15} (\frac{D_B}{a})^{22/15} (\frac{D_A}{a})^{-2/3} \tag{20}$$

With accuracy of the logarithmic prefactor, volume fraction profile $c_A(r)$ in the corona of starlike micelle is given by

$$c_A(r) \simeq Q^{2/3} \left(\frac{a}{r}\right)^{4/3} \left(\frac{a}{D_A}\right)^{2/3} n_A \simeq ({\tau_B}^2 N_B)^{8/15} \left(\frac{a}{r}\right)^{4/3} (\frac{D_A}{a})^{-2/3} n_A \tag{21}$$

with thickness D_A of bb block A specified by eq 4. $c_A(r)$ is regulated by the solvent selectivity for the B-block (τ_B), size $D_A(n_A)$ of superblob in soluble

block A, DP N_B of condensed block B, but does not exhibit power law dependence on DP n_B of side chains in block B.

As it follows from eq 17, the thickness of micelle corona depends on DP n_A of the side chain in soluble block A. Different modes of branching, e.g., an increase in n_A at fixed $N_A = M_A n_A$ or fixed M_A would lead to the respective decrease or increase in the corona thickness, H, at almost constant value of the aggregation number, Q. The effect of n_B is weak, and manifests itself only *via* logarithmic dependences in eqs 18,16. This situation changes upon decreasing N_B.

3.1 Starlike micelles with $M_B \leq M_B^*$

The bb branching and thickness $D_B \simeq a(n_B/\tau_B)^{1/2}$ of the core-forming block B manifest themselves at relatively small values of N_B. According to eq 19, a decrease in N_B leads to the decrease in the core/corona interface area s per molecule. Area s becomes equal to the cross-section of superblob of either block A (if $D_A \geq D_B$, that is, $n_A \geq n_B$) or block B (if $D_B \geq D_A$, that is, $n_B \geq n_A$) when

$$N_B = N_B^* \simeq \tau_B^3 \left\{ \begin{array}{ll} \left(\frac{D_A}{a}\right)^5 & D_A \geq D_B \\ \left(\frac{D_B}{a}\right)^5 & D_B \geq D_A \end{array} \right.$$

or, equivalently,

$$M_B = M_B^* \simeq \tau_B^2 \left\{ \begin{array}{ll} \left(\frac{D_A}{a}\right)^3 \left(\frac{D_A}{D_B}\right)^2 & D_A > D_B \\ \left(\frac{D_B}{a}\right)^3 & D_B > D_A \end{array} \right. \tag{22}$$

A decrease in $M_B \leq M_B^*$ would perturb the equilibrium structure of superblobs leading to the increase in their "internal" free energy.

3.1.1 Block copolymers with $D_B \gg D_A$

In this case $M_B^* \simeq \tau_B^2 \, (D_B/a)^3$, and at $M_B = M_B^*$ the backbones of core blocks B approach maximal extension, $R/aM_B \simeq 1$. If at $M_B \leq M_B^*$ the aggregation number Q would follow eq 16, then the average volume fraction $\overline{c}_B$ of monomer units in the core with radius $R \simeq aM_B$ would increase as

$$\overline{c}_B \simeq \frac{QN_B}{M_B^3} \simeq \tau_B \left(\frac{M_B^*}{M_B}\right)^{6/5} \geq \tau_B$$

and ternary monomer-monomer interactions with the third virial coefficient $wa^3 \simeq a^3$ would increase the free energy of block B by

$$\delta F_B/k_BT \simeq wN_B \left(\overline{c}_B\right)^2 \simeq M_B D_B^2 \tau_B^3 \left(M_B^*/M_B\right)^{12/5}$$

Comparison of δF_B to the conformation free energy per chain, $F/k_BT \simeq \tau_B^2 D_B^2$, at $s \simeq D_B^2$ indicates that $\delta F_B \gg F$, and therefore aggregation number Q varies according to a different power law dependence at $M_B \leq M_B^*$.

In this range of M_B, the increase in "internal" free energy of the core superblobs upon compression prevents the decrease in area s below D_B^2, keeping

$$s \simeq D_B^2 \tag{23}$$

As a result, radius R of micelle core decreases at $M_B \leq M_B^*$ as

$$R/a \simeq \frac{a^3 N_B}{s\tau_B} \simeq \frac{N_B}{\tau_B}\left(\frac{a}{D_B}\right)^2 \simeq M_B \tag{24}$$

and aggregation number Q drops as

$$Q \simeq \frac{R^3\tau_B}{a^3 N_B} \simeq \left(\frac{N_B}{\tau_B}\right)^2 \left(\frac{a}{D_B}\right)^6 \simeq \left(\frac{aM_B}{D_B}\right)^2 \tag{25}$$

while corona thickness H yields

$$H/a \simeq \left(\frac{D_A}{a}\right)^{2/5} M_A^{3/5} Q^{1/5} \simeq M_A^{3/5} M_B^{2/5} \left(\frac{D_A}{D_B}\right)^{2/5} \tag{26}$$

Disintegration of micelles in unimers ($Q \simeq 1$) occurs when

$$M_B \simeq D_B/a \tag{27}$$

which corresponds to one superblob per core block B.

We emphasize that at $M_B \leq M_B^*$ the conformation free energy F per molecule is dominated by the surface free energy,

$$\frac{F}{k_BT} \simeq \frac{F_{A/B}}{k_BT} \simeq \frac{s}{\xi_t^2} \simeq \tau_B^2 \frac{s}{a^2} \simeq \tau_B^2 \left(\frac{D_B}{a}\right)^2 \tag{28}$$

which is preserved constant due to "internal" free energy of core superblobs. The conformation free energy of A- blocks,

$$\frac{F_A}{k_BT} \simeq Q^{1/2} \simeq \frac{N_B}{\tau_B}\left(\frac{a}{D_B}\right)^3 \leq \frac{F_{A/B}}{k_BT} \tag{29}$$

and

$$\frac{F_B}{k_BT} \simeq \frac{R^2}{D_B^2 N_{BS}} \simeq \frac{N_B}{\tau_B}\left(\frac{a}{D_B}\right)^3 \simeq \frac{F_A}{k_BT} \tag{30}$$

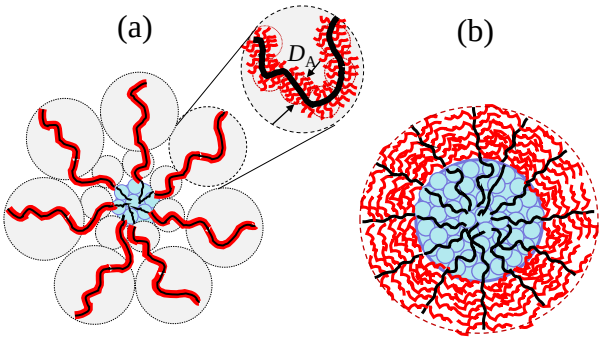

Figure 3: Schematic of (a) starlike micelle with $D_B \gg D_A$ and strongly stretched backbones of core blocks (regime ST_B in the diagram of states in Figure 5)., and (b) crew-cut micelle with strongly stretched backbones in laterally compressed corona blocks (regimes CC^2, $\mathrm{CC}_{A,B}$ in the digaram of states in Figure 7

Notably, the backbones of blocks B remain strongly stretched at all $M_B \leq M_B^*$. The number of superblobs, $N_{BS} \simeq aM_B/D_B$, reduces upon decreasing $N_B = M_B n_B$, and disintegration of micelles in unimers ($Q \simeq 1$) occurs when block B reduces to a single superblob. We refer to such self-assemblies as starlike core-stretched (ST_B) micelles (see schematic in **Figure 3a**).

As it follows from eqs 24 and 26, ST_B micelles remain starlike with $H \geq R$ if

$$M_A \geq M_B \left(\frac{D_A}{D_B}\right)^{2/3} \tag{31}$$

3.1.2 Block copolymers with $D_A \gg D_B$

In this case

$$M_B^* \simeq \tau_B^2 \left(\frac{D_A}{a}\right)^3 \left(\frac{D_A}{D_B}\right)^2 \tag{32}$$

and at $M_B \leq M_B^*$ perturbation of the corona superblobs occurs in a spherical layer with inner radius R and outer radius $r^* \simeq D_A Q^{1/2}$. At $r = r^* \simeq D_A Q^{1/2}$, the area per chain $s(r^*) \simeq H^{*2}/Q = D_A^2$, and the rest of corona superblobs located at $r \geq r^*$ remain unperturbed. The chain segments in the perturbed layer have totally stretched backbones with DP (r^*/a), and volume fraction $c_A(r)$ of monomer units at distance r from the core center yields

$$c_A(r) \simeq \frac{Q n_A a^2}{r^2}, \qquad r \leq r^*$$

The increase in "internal" free energy, δF_A , of laterally compressed corona superblobs can be estimated *via* osmotic pressure $\pi(r)$ in a semi-dilute solution of side chains with volume fraction $c_A(r)$,

$$\frac{\pi(r)a^3}{k_B T} \simeq c_A(r)^{\frac{3\nu}{3\nu-1}} \simeq \left(\frac{Q n_A a^2}{r^2}\right)^{\frac{3\nu}{3\nu-1}}$$

where $\nu \approx 3/5$ or $\nu = 1/2$ under good or theta-solvent conditions for the A-block and

$$\frac{\delta F_A}{k_B T} \simeq \frac{1}{Q}\int_R^{r^*} \frac{\pi(r)a^3}{k_B T} r^2 dr \simeq \frac{(Q n_A)^{\frac{3\nu}{3\nu-1}}}{Q}\left[\left(\frac{a}{R}\right)^{\frac{3-3\nu}{3\nu-1}} - \left(\frac{a}{h^*}\right)^{\frac{3-3\nu}{3\nu-1}}\right] \qquad (33)$$

By substituting $R \simeq a^3(N_B/s\tau_B) \simeq a M_B D_B^2/s$, $Q \simeq R^2/s$, $r^* \simeq D_A Q^{1/2}$, $n_A \simeq (D_A/a)^{\frac{\nu+1}{2\nu}}$ (eq 4 with $\tau_A \simeq 1$), and dimensionless ratio $x = D_A^2/s$ in eq 33, one estimates the increase in the free energy of perturbed layer per molecule as

$$\frac{\delta F_A}{k_B T} \simeq M_B \left(\frac{a}{D_A}\right)^{3/2}\left(\frac{D_B}{a}\right)^2\left(x^{\frac{3\nu}{(3\nu-1)}} - x^{\frac{3}{2}}\right)$$

Minimization of the sum of dominant contributions to the diblock free energy,

$$\frac{\delta F_A}{k_B T} + \frac{F_{A/B}}{k_B T} \simeq M_B \left(\frac{a}{D_A}\right)^{3/2}\left(\frac{D_B}{a}\right)^2\left(x^{\frac{3\nu}{(3\nu-1)}} - x^{\frac{3}{2}}\right) + \tau^2\left(\frac{D_A}{a}\right)^2\frac{1}{x},$$

with respect to x (i.e., with respect to s) gives

$$s = \frac{D_A^2}{x} \simeq \begin{cases} D_A^2 & \text{if } M_B \gg M_B^{**} \\ a^2\left(\frac{D_A}{a}\right)^{\frac{3(\nu+1)}{2(6\nu-1)}}\left(\frac{M_B D_B^2}{\tau_B^2 a^2}\right)^{\frac{3\nu-1}{6\nu-1}} & \text{if } M_B \ll M_B^{**} \end{cases} \qquad (34)$$

with

$$M_B^{**} \simeq \tau_B^2\left(\frac{D_A}{a}\right)^{3/2}\left(\frac{D_A}{D_B}\right)^2 \qquad (35)$$

The first line in eq 34 ($x \simeq 1$) corresponds to constant area $s \simeq D_A^2$ at $M_B^* \gg M_B \gg M_B^{**}$ (regime ST^1 in Figure 7), with the equilibrium parameters of micelles

$$R/a \simeq \frac{a^3 N_B}{s\tau_B} \simeq M_B \left(\frac{D_B}{D_A}\right)^2, \tag{36}$$

$$Q \simeq \frac{R^2}{s} \simeq M_B^2 \left(\frac{D_B}{a}\right)^4 \left(\frac{a}{D_A}\right)^6, \tag{37}$$

and

$$H/a \simeq \left(\frac{D_A}{a}\right)^{2/5} M_A^{3/5} Q^{1/5} \simeq M_A^{3/5} M_B^{2/5} \left(\frac{D_B}{D_A}\right)^{4/5} \tag{38}$$

In this range of $M_B^{**} \leq M_B \leq M_B^*$ (regime ST^1 in the diagram states in Figure 7), the core radius decreases as $R/a \sim M_B$ with $r^* \simeq R$. According to eqs 36 and 38, starlike micelles transform in crew-cut aggregates ($H \simeq R$) when

$$M_A \simeq M_B \left(\frac{D_B}{D_A}\right)^2 \tag{39}$$

According to the second line in eq 34, at $M_B \leq M_B^{**}$ (regime ST^2 in Figure 7)

$$R/a \simeq \frac{a^2 N_B}{\tau_B s} \simeq \left(M_B \frac{D_B^2}{a^2}\right)^{\frac{3\nu}{6\nu-1}} \tau_B^{\frac{2(3\nu-1)}{6\nu-1}} \left(\frac{D_A}{a}\right)^{-\frac{3(\nu+1)}{2(6\nu-1)}} \tag{40}$$

$$Q \simeq \frac{R^2}{s} \simeq \left(M_B \frac{D_B^2}{a^2}\right)^{\frac{3\nu+1}{6\nu-1}} \tau_B^{\frac{6(3\nu-1)}{6\nu-1}} \left(\frac{D_A}{a}\right)^{-\frac{9(\nu+1)}{2(6\nu-1)}} \tag{41}$$

$$H/a \simeq \left(\frac{D_A}{a}\right)^{2/5} M_A^{3/5} Q^{1/5} \tag{42}$$

According to eq 42, a decrease in M_A leads to full stretching of the corona backbones ($H \simeq aM_A$) while micelles are still starlike, at

$$M_A \simeq \left(M_B \frac{D_B^2}{a^2}\right)^{\frac{3\nu+1}{2(6\nu-1)}} \tau_B^{\frac{3(3\nu-1)}{6\nu-1}} \left(\frac{D_A}{a}\right)^{-\frac{15\nu-13}{4(6\nu-1)}} \tag{43}$$

This boundary is shown by the dashed line in regime ST^2 in Figure 7.

Transition to crew-cut aggregates ($R/a \simeq M_A$) occurs when

$$M_A \simeq \left(M_B \frac{D_B^2}{a^2}\right)^{\frac{3\nu}{(6\nu-1)}} \tau_B^{\frac{2(3\nu-1)}{6\nu-1}} \left(\frac{D_A}{a}\right)^{-\frac{3(\nu+1)}{2(6\nu-1)}} \tag{44}$$

Upon a decrease in $s \leq D_B^2$ (regime ST_B in Figure 7), that starts at

$$M_B = M_B^{***} \simeq \tau_B^2 \left(\frac{D_B}{a}\right)^{\frac{6\nu}{3\nu-1}} \left(\frac{D_A}{a}\right)^{-\frac{3(\nu+1)}{2(3\nu-1)}} \tag{45}$$

the equilibrium parameters of micelles are described by eqs 23-27 in the previous subsection. That is,

$$R \simeq aM_B \tag{46}$$

$$Q \simeq \left(\frac{aM_B}{D_B}\right)^2 \tag{47}$$

$$H/a \simeq M_A^{3/5} M_B^{2/5} \left(\frac{D_A}{D_B}\right)^{2/5} \tag{48}$$

The backbones of the corona A-blocks approach maximal extension ($H \simeq aM_A$) when micelles are still starlike, at

$$M_A \simeq M_B \left(\frac{D_A}{D_B}\right) \tag{49}$$

indicated by the dashed line in regime ST_B in Figure 7.

According to eq 46, transition to crew-cut aggregates ($R/a \simeq M_A$) occurs when

$$M_A \simeq M_B \tag{50}$$

For symmetrically branched blocks with $D_A = D_B$, eqs 23-26 coincide with eqs 34-38.

4 Crew-cut micelles with $M_B \geq M_B^*$

Starlike micelles with $H \geq R$ transform in crew-cut aggregates with $H \leq R$, when $H \simeq R$. For block copolymers with $M_B \geq M_B^*$, eqs 18 and 17 specify the boundary between starlike and crew-cut micelles as

$$M_A \simeq \tau_B^{8/15} M_B^{11/15} \left(\frac{D_B}{a}\right)^{22/15} \left(\frac{D_A}{a}\right)^{-2/3} \tag{51}$$

In a crew-cut micelle, corona is planar-like, and its conformation free energy F_A can be obtained from the free energy $F/k_BT \simeq N_A(s/a^2)^{-\frac{1}{2\nu}}$ in a planar

brush of linear chains with DP N_A and grafting area s by substitution $a \to D_A$, $N_A \to N_{AS} = aM_A/D_A$, and $\nu = 3/5$, to give

$$\frac{F_A}{k_BT} \simeq M_A \left(\frac{D_A}{a}\right)^{2/3} \left(\frac{a^2}{s}\right)^{5/6} \tag{52}$$

By balancing $F_A \simeq F_{A/B}$, one finds

$$\frac{s}{a^2} \simeq \left(\frac{D_A}{a}\right)^{4/11} M_A^{6/11} \tau_B^{-12/11} \tag{53}$$

aggregation number

$$Q \simeq \frac{R^2}{s} \simeq \frac{M_B^2 \tau_B^{38/11}}{M_A^{18/11}} \left(\frac{D_B}{a}\right)^4 \left(\frac{D_A}{a}\right)^{-12/11} \tag{54}$$

core radius

$$R/a \simeq \frac{N_B \tau_B^{1/11}}{M_A^{6/11}} \left(\frac{a}{D_A}\right)^{4/11} \simeq \frac{M_B \tau_B^{13/11}}{M_A^{6/11}} \left(\frac{D_B}{a}\right)^2 \left(\frac{a}{D_A}\right)^{4/11} \tag{55}$$

corona thickness

$$H/a \simeq M_A \left(\frac{D_A^2}{s}\right)^{1/3} \simeq \left(\frac{D_A}{a}\right)^{6/11} M_A^{9/11} \tau_B^{4/11} \tag{56}$$

and the equilibrium free energy of corona block,

$$\left(\frac{F_A}{k_BT}\right) \simeq \tau_B^2 \left(\frac{s}{a^2}\right) \simeq \left(\frac{D_A}{a}\right)^{4/11} M_A^{6/11} \tau_B^{10/11} \tag{57}$$

As it follows from eqs 55 and 56, a decrease in M_A leads to the increase in the core radius R, and the decrease in the corona thickness, H.

4.1 Crew-cut micelles with $M_B \ll M_B^*$

4.1.1 Block copolymers with $D_B \gg D_A$

If $D_B \geq D_A$, a decrease in M_A leads first to $s \simeq D_B^2$ which happens at

$$M_A^* \simeq \tau_B^2 \left(\frac{D_B}{a}\right)^3 \left(\frac{D_B}{D_A}\right)^{2/3}$$

At smaller $M_A \leq M_A^*$, interfacial area per molecule remains constant, $s \simeq D_B^2$, and crew-cut aggregates have strongly stretched core blocks with

$$R \simeq aM_B \tag{58}$$

and extended corona blocks with

$$H \simeq aM_A \left(\frac{D_A^2}{s}\right)^{1/3} \simeq aM_A \left(\frac{D_A}{D_B}\right)^{2/3} \tag{59}$$

The boundary $R \simeq H$ or, equivalently, $M_A \simeq M_B \left(D_B/D_A\right)^{2/3}$separates crew-cut micelles from starlike (see also eq 31).

4.1.2 Block copolymers with $D_A \gg D_B$

In this scenario, a decrease in M_A leads first to $s \simeq D_A^2$, which happens at

$$M_A^* \simeq \tau_B^2 \left(\frac{D_B}{a}\right)^3 \tag{60}$$

At $M_A = M_A^*$, backbones in the corona blocks approach maximal extension, $H(M_A^*) \simeq aM_A^*$. At smaller $M_A \leq M_A^*$, $H \simeq aM_A$, and the corona conformation free energy

$$\frac{F_A}{k_BT} \simeq \frac{aM_A}{D_A} \tag{61}$$

while

$$R/a \simeq M_B \left(\frac{D_B}{D_A}\right)^2 \tag{62}$$

and

$$Q \simeq \frac{R^2}{s} \simeq M_B^2 \left(\frac{D_B}{a}\right)^4 \left(\frac{a}{D_A}\right)^6$$

This regime (CC_A^1 in the diagram of states in Figure 7) lasts until M_A decreases down to

$$M_A^{**} \simeq \tau_B^2 \left(\frac{D_A}{a}\right)^{3/2} \tag{63}$$

At this point, the "internal" free energy of unperturbed corona superblobs reduces to the surface free energy, F_{AB}. Further decrease in $M_A \leq M_A^{**}$ leads to the decrease in s, and concomitant increase in the average volume fraction $c_A = a^2 n_A/s$ of monomer units in the corona, leading to the increase δF_A in the "internal" free energy of compressed corona superblobs per molecule,

$$\frac{\delta F_A}{k_BT} \simeq M_A n_A c_A^{\frac{1}{3\nu-1}} \simeq M_A n_A \left(\frac{a^2 n_A}{s}\right)^{\frac{1}{3\nu-1}}$$

with $n_A \simeq (D_A/a)^{\frac{\nu+1}{2\nu}}$(eq 4 at $\tau_A \simeq 1$).

The equilibrium parameters of crew-cut micelles at $M_A \ll M_A^{**}$ (regime CC_A^2 in Figure 7) can be found by balancing $\delta F_A \simeq F_{A/B}$ to give

$$\frac{s}{a^2} \simeq \left(\frac{D_A}{a}\right)^{\frac{\nu+1}{2\nu}} \left(\frac{M_A}{\tau_B^2}\right)^{\frac{(3\nu-1)}{3\nu}} \tag{64}$$

In regime CC_A^2 the core radius

$$R/a \simeq \frac{M_B D_B^2}{s} \simeq M_B \left(\frac{D_B}{a}\right)^2 \left(\frac{D_A}{a}\right)^{-\frac{\nu+1}{2\nu}} \left(\frac{\tau_B^2}{M_A}\right)^{\frac{(3\nu-1)}{3\nu}} \tag{65}$$

the aggregation number

$$Q \simeq \frac{R^2}{s} \simeq M_B^2 \left(\frac{D_B}{a}\right)^4 \left(\frac{D_A}{a}\right)^{-\frac{3(\nu+1)}{2\nu}} \left(\frac{\tau_B^2}{M_A}\right)^{\frac{(3\nu-1)}{\nu}}$$

the corona thickness

$$H/a \simeq M_A \tag{66}$$

while the free energy per corona block

$$\frac{F_A}{k_B T} \simeq \tau_B^2 \frac{s}{a^2} \simeq \tau_B^{\frac{2}{3\nu}} \left(\frac{D_A}{a}\right)^{\frac{\nu+1}{2\nu}} M_A^{\frac{(3\nu-1)}{3\nu}}$$

Area s drops down to $s \simeq D_B^2$ when M_A decreases to

$$M_A^{***} \simeq \tau_B^2 \left(\frac{D_B}{a}\right)^{\frac{6\nu}{3\nu-1}} \left(\frac{D_A}{a}\right)^{-\frac{3(\nu+1)}{2(3\nu-1)}} \tag{67}$$

at which point backbones of the core blocks approach maximal extension, $R \simeq aM_B$ (see schematic in **Figure 3b**)

At lower values of $M_A \ll M_A^{***}$(regime $CC_{A,B}$ in Figure 7), $s \simeq D_B^2$, and crew-cut aggregates have strongly stretched both core and corona backbones, $R \simeq aM_B$, $H \simeq aM_A$, and

$$\frac{F_A}{k_B T} \simeq M_A n_A \left(\frac{a^2 n_A}{D_B^2}\right)^{\frac{1}{3\nu-1}} \simeq M_A \left(\frac{D_A}{a}\right)^{\frac{3(\nu+1)}{2(3\nu-1)}} \left(\frac{D_B}{a}\right)^{-\frac{2}{3\nu-1}}$$

with boundary

$$M_A \simeq M_B \tag{68}$$

between starlike and crew-cut micelles.

5 Discussion

The developed scaling model of spherical micelles with bb branched core and corona blocks is based on subdivision of the bottlebrush free energy in the "internal" free energy of superblobs and the free energy of superblob-superblob interactions. The former contribution accounts for monomer-monomer interactions within superblobs (on length scales smaller than D_i, $i = A, B$) and is much larger than k_BT per superblob. The latter contribution governs the chain conformations on length scales larger than D_i, and approaches k_BT per superblob only in fully stretched or collapsed chains of superblobs. If the structure of superblobs is unperturbed in the core and corona domains, the "internal" contribution does not manifest itself in micellization of diblock copolymer with bb blocks. Perturbation (compression) of the core superblobs is always counteracted by the increase in "internal" free energy of globular core, preserving $s \simeq D_B^2$, giving rise to micelles with strongly stretched backbones of the core blocks. Perturbation of the corona superblobs prevents the decrease in $s < D_A^2$ in micelles with $D_A \geq D_B$ only in a limited interval of $M_A^{**} \leq M_A \leq M_A^*$.

To elucidate the effect of bb branching of blocks A and B on the equilibrium properties of micelles, we start with brief review of the diagram of states for AB block copolymers with linear blocks.

In **Figure 4** we present scaling-type diagram of states in M_A,M_B log-log coordinates for AB copolymer with linear blocks ($\tau_A = 1$). It comprises regime ST of starlike micelles, regime CC of crew-cut micelles, and the sediment accumulating lamellar aggregates after morphological transformations sphere-to-cylinder-to-lamella. The corridor of stability for cylindrical (wormlike) micelles is not distinguished in scaling terms.[45] Both boundaries of the corridor are specified by same scaling dependences, $M_A \simeq M_B^{\frac{1+2\nu}{11\nu}} \tau_B^{\frac{8\nu-7}{11\nu}}$, with different numerical coefficients and are indicated by dotted line in Figure 4. Power law dependences for micelle parameters are collected in **Table 1**.

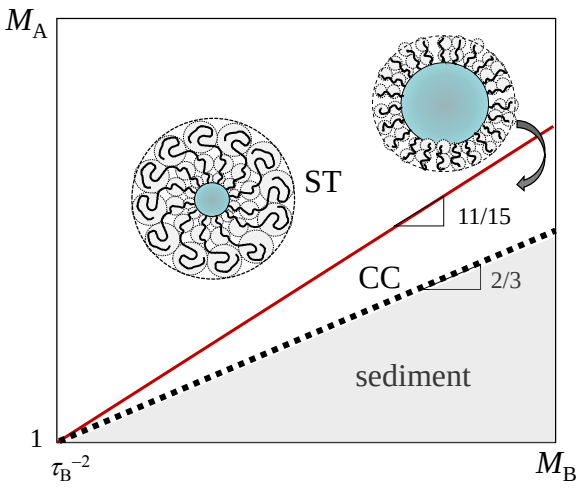

Figure 4: Scaling-type diagram of states for AB diblock copolymer micelles with linear blocks in good solvent.[45,48] M_A and M_B are the respective DPs of soluble and insolube linear blocks, $\nu = 3/5, \tau_A = 1$. The values of other parameters are $L_A/a = 1, \gamma = \tau_B^2, \phi_B = \tau_B$. Dotted line with slope 2/3 marks the stability corridor of cylindrical micelles.

Table 1. *Power law dependences for parameters of spherical micelles formed by AB copolymer with linear core and corona blocks with respective DP M_B and M_A.*[12,13] $\tau_A = 1$.

Regime	Q	R/a	H/a
ST	$\tau_B^{8/5} M_B^{4/5}$	$\tau_B^{1/5} M_B^{3/5}$	$M_A^{\nu} (\tau_B^2 M_B)^{\frac{2(1-\nu)}{5}}$
CC	$\tau_B^{\frac{8\nu-2}{2\nu+1}} M_B^2 M_A^{-\frac{6\nu}{2\nu+1}}$	$\tau_B^{\frac{2\nu-1}{2\nu+1}} M_B M_A^{-\frac{2\nu}{2\nu+1}}$	$\tau_B^{\frac{2-2\nu}{2\nu+1}} M_A^{\frac{3\nu}{2\nu+1}}$

Table 2. *Power law dependences for parameters of spherical micelles with $D_B \geq D_A$ in Figure 6.*

Regime	Q	R/a	H/a
ST	${\tau_B}^{8/5} N_B^{4/5}$	$\tau_B^{1/5} N_B^{3/5}$	$a M_A^{3/5} (D_A/a)^{2/5} ({\tau_B}^2 N_B)^{4/25}$
ST_B	$(a M_B/D_B)^2$	M_B	$M_A^{3/5} M_B^{2/5} (D_A/D_B)^{2/5}$
CC	$\frac{M_B^2 \tau_B^{38/11}}{M_A^{18/11}} \left(\frac{D_B}{a}\right)^4 \left(\frac{D_A}{a}\right)^{-12/11}$	$\frac{M_B \tau_B^{13/11}}{M_A^{6/11}} \left(\frac{D_B}{a}\right)^2 \left(\frac{D_A}{a}\right)^{-4/11}$	$(D_A/a)^{6/11} M_A^{9/11} \tau_B^{4/11}$

Table 3. *Power law dependences for boundaries between regimes in Figure 6.*

Regimes	*Boundaries*
$ST - CC$	$M_A \simeq M_B^{11/15} \tau_B^{8/15} \left(\frac{D_B}{a}\right)^{22/15} \left(\frac{D_A}{a}\right)^{-2/3}$
$ST - ST_B$	$M_B = M_B^* \simeq \tau_B^2 \left(D_B/a\right)^3$
$ST_B - CC$	$M_A \simeq M_B \left(D_B/D_A\right)^{2/3}$

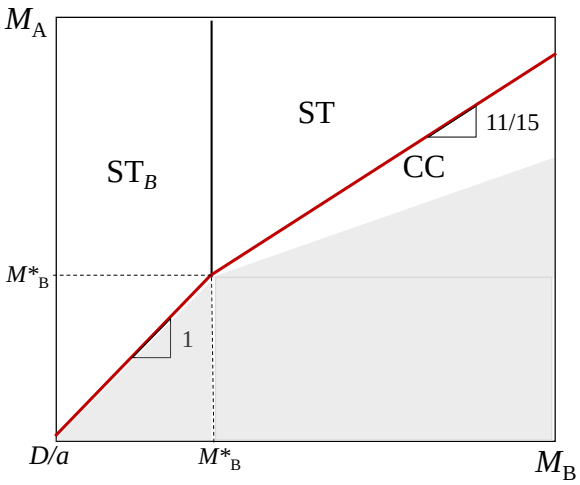

Figure 5: Scaling-type diagram of states for AB diblock copolymer micelles with symmetrically branched bb blocks, log-log coordinates. $D_B = D_A = D, M_B^* = \tau_B^2 (D/a)^3$. At Y-axis ($M_B = D/a$) micelles disintegrate in unimers. In shaded area (shown schematically) spherical micelles change morphology sphere to-cylinder-to-lamella with subsequent precipitation in the sediment.

In Figure 5 we present scaling-type diagram for micelles formed by AB copolymer with symmetrically branched blocks, $D_A = D_B = D$. Compared to the diagram in Figure 4, it comprises additional regime ST_B located at relatively small values of $M_B \leq M_B^* \simeq \tau_B^2 (D/a)^3$ at which the backbones in core blocks are strongly stretched approaching maximal extension, $R = aM_B$ (see schematic in **Figure 3a**).

In **Figure 6** we present scaling-type diagram for micelles with asymmetrically branched blocks, $D_B \geq D_A$. Such branching asymmetry does not leads to additional regimes in the diagram of states but merely shifts all the boundaries to larger values of M_A. The equilibrium micelle parameters, Q, R, and H, in various regimes in Figure 6 are collected in **Table 2**. The boundaries between the regimes are presented in **Table 3**.

In **Figure 7** we present the scaling-type diagram of states for AB block copolymers with $D_A \geq D_B$. In this case, the diagram contains a number of additional regimes ($ST^1, ST^2, CC_A^1, CC_A^2, CC_{A,B}$) that are not present in

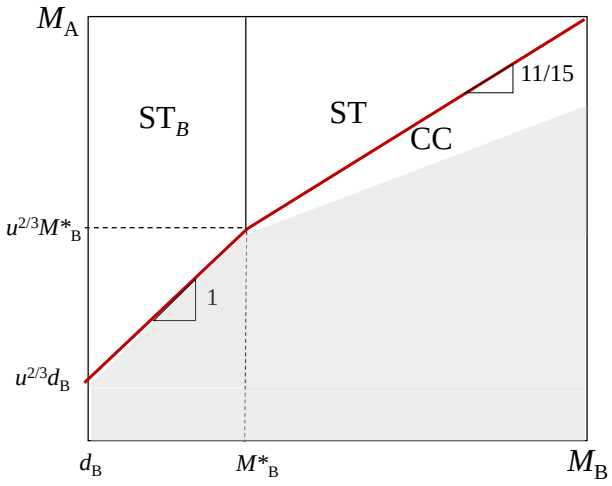

Figure 6: Scaling-type diagram of states for AB diblock copolymer micelles with asymmetrically branched blocks. $D_B \geq D_A, u = D_B/D_A \geq 1, M_B^* = \tau_B^2(D_B/a)^3$. In shaded area (shown schematically) spherical micelles change morphology sphere to-cylinder-to-lamella with subsequent precipitation in the sediment.

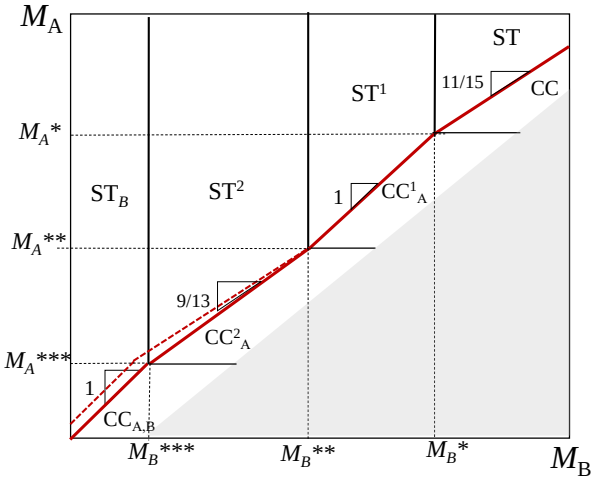

Figure 7: Scaling-type diagram of states for AB diblock copolymer micelles with asymmetrically branched bb blocks, $D_B \leq D_A$ in athermal solvent, $\nu = 3/5$. M_A^*, M_A^{**}, and M_A^{***} are given by eqs 60, 63,67, respectively. M_B^*, M_B^{**}, and M_B^{***} are given by eqs 32, 35,45, respectively. On the dashed line backbones in corona blocks of starlike micelles approach maximal extension, $H = aM_A$. In shaded area (shown schematically) spherical micelles change morphology sphere-to-cylinder-to-lamella with subsequent precipitation in the sediment.

figure 6. Dashed lines in regimes ST^2 and ST_B indicate the approach to full stretching of the backbones in corona blocks, $H = aM_A$(eqs 43 and 49), which happens when micelles are still starlike. In these regimes, A-blocks in the coronae of micelles are laterally compressed. Power law dependences for micelle parameters in different regimes of the diagram of states in Figure 7 are collected in **Table 4** and **Table 5** with boundaries in **Table 6**.

Although the predicted exponents require asymptotically large values of DPs of backbones and side chains, the power law dependences in Tables 2 and 4 predict the trends in micelles behavior, and could serve as guidelines to manipulate the properties of spherical micelles by changing architecture of the blocks. As it follows from Tables 2 and 4, branching of the blocks at fixed values of M_A and M_B manifests itself in additional dependences of micelle parameters on D_A and D_B, that is, on the DPs n_A and n_B of side chains. While variations in $n_A \sim (D_A/a)^{\frac{1+\nu}{2\nu}}$ lead to the power law dependences in micelle parameters and positions of boundaries, variations in $n_B \simeq \tau_B (D_B/a)^2$ manifest themselves in either weak logarithmic dependence in regime ST (*via* prefactor omitted in Tables 2 and 4), or at relatively small values of $M_B < M_B^*$.

It should be emphasized that in certain regions of the diagram of states the conditions $M_A > D_A/a$ and $M_B > D_B/a$, ensuring bb type of blocks branching could be violated. In these regions the blocks become starlike, and the power law dependences for micelle parameters in these regions should be changed correspondingly. Such regions are indicated by shaded areas in Figure 8.

Table 4. *Power law dependences for aggregation number Q of spherical micelles with* $D_A \geq D_B$ in *Figure 7.*

Regime	Q
ST	${\tau_B}^{8/5} N_B^{4/5}$
ST^1	$M_B^2 \left(\frac{D_B}{a}\right)^4 \left(\frac{a}{D_A}\right)^6$
ST^2	$\left(M_B \frac{D_B^2}{a^2}\right)^{\frac{3\nu+1}{6\nu-1}} \tau_B^{\frac{6(3\nu-1)}{6\nu-1}} \left(\frac{a}{D_A}\right)^{\frac{12\nu}{6\nu-1}}$
ST_B	$\left(aM_B/D_B\right)^2$
CC	$\frac{M_B^2 \tau_B^{38/11}}{M_A^{18/11}} \left(\frac{D_B}{a}\right)^4 \left(\frac{a}{D_A}\right)^{12/11}$
CC_A^1	$M_B^2 \left(\frac{D_A}{a}\right)^{-6} \left(\frac{D_B}{a}\right)^4$
CC_A^2	$M_B^2 \left(\frac{D_B}{a}\right)^4 \left(\frac{D_A}{a}\right)^{-\frac{3(\nu+1)}{2\nu}} \left(\frac{\tau_B^2}{M_A}\right)^{\frac{(3\nu-1)}{\nu}}$
$CC_{A,B}$	$\left(aM_B/D_B\right)^2$

Table 5. *Power law dependences for core radius R and corona thickness H of spherical micelles with* $D_A \geq D_B$ in *Figure 7.*

Regime	R/a	H/a
ST	$\tau_B^{1/5} N_B^{3/5}$	$aM_A^{3/5}(D_A/a)^{2/5}(\tau_B^2 N_B)^{4/25}$
ST^1	$M_B \left(\frac{D_B}{D_A}\right)^2$	$M_A^{3/5} M_B^{2/5} \left(\frac{D_B}{D_A}\right)^{4/5}$
ST^2	$\left(M_B \frac{D_B^2}{a^2}\right)^{\frac{3\nu}{6\nu-1}} \tau_B^{\frac{2(3\nu-1)}{6\nu-1}} \left(\frac{a}{D_A}\right)^{\frac{4\nu}{6\nu-1}}$	$\left(\frac{D_A}{a}\right)^{2/5} M_A^{3/5} Q^{1/5}$, M_A
ST_B	M_B	$M_A^{3/5} M_B^{2/5} \left(\frac{D_A}{D_B}\right)^{2/5}$
CC	$\frac{M_B \tau_B^{13/11}}{M_A^{6/11}} \left(\frac{D_B}{a}\right)^2 \left(\frac{a}{D_A}\right)^{4/11}$	$\left(\frac{D_A}{a}\right)^{6/11} M_A^{9/11} \tau_B^{4/11}$
CC_A^1	$M_B(\frac{D_B}{D_A})^2$	M_A
CC_A^2	$M_B \left(\frac{D_B}{a}\right)^2 \left(\frac{D_A}{a}\right)^{-\frac{\nu+1}{2\nu}} \left(\frac{\tau_B^2}{M_A}\right)^{\frac{(3\nu-1)}{3\nu}}$	M_A
$CC_{A,B}$	M_B	M_A

Table 6. *Power law dependences for boundaries between regimes in Figure 7.*

Regimes	*Boundaries*
$ST-CC$	$M_A \simeq M_B^{11/15}\tau_B^{8/15}\left(\frac{D_B}{a}\right)^{22/15}\left(\frac{D_A}{a}\right)^{-2/3}$
$ST-ST^1$	$M_B \simeq \tau_B^2\left(\frac{D_A}{a}\right)^3(D_A/D_B)^2$
ST^1-ST^2	$M_B \simeq \tau_B^2\left(\frac{D_A}{a}\right)^{\frac{2\nu}{3\nu-1}}(D_A/D_B)^2$
ST^2-ST_B	$M_B \simeq \tau_B^2\left(\frac{D_B}{a}\right)^{\frac{6\nu}{3\nu-1}}\left(\frac{D_A}{a}\right)^{-\frac{4\nu}{3\nu-1}}$
$CC-CC_A^1$	$M_A \simeq \tau_B^2\left(\frac{D_A}{a}\right)^3$
$CC_A^1-CC_A^2$	$M_A \simeq \tau_B^2\left(\frac{D_A}{a}\right)^{\frac{3}{2}}$
$CC_A^2-CC_{B,A}$	$M_A \simeq \tau_B^2\left(\frac{D_B}{a}\right)^{\frac{6\nu}{3\nu-1}}\left(\frac{D_A}{a}\right)^{-\frac{4\nu}{3\nu-1}}$
$CC_{B,A}-ST_B$	$M_A \simeq M_B$
$CC_A^2-ST^2$	$M_A \simeq \left(M_B\frac{D_B^2}{a^2}\right)^{\frac{3\nu}{(6\nu-1)}}\tau_B^{\frac{2(3\nu-1)}{6\nu-1}}\left(\frac{D_A}{a}\right)^{-\frac{4\nu}{6\nu-1}}$
$CC_A^1-ST^1$	$M_A \simeq M_B(D_B/D_A)^2$

5.1 Critical micelle concentration (CMC)

Similarly to the case of linear block copolymers,[47,48] critical micelle concentration (CMC) for diblock copolymer with bb branched blocks is governed mostly by DP N_B of insoluble block B while the dependence on DP $N_A$of soluble block A is weak. In scaling terms, CMC for spherical micelles with $Q \gg 1$ is determined by the surface free energy of unimer with condensed block B as

$$\ln CMC \simeq -(\tau_B^2 N_B)^{2/3} + F_A/k_BT \tag{69}$$

and is not sensitive to bb branching of block B with fixed total DP $N_B \approx M_B n_B$. The free energy F_A per corona block is always much smaller that the surface free energy of unimer (first term in eq 69). The dependence of F_A on architecture of the blocks varies from one regime in the diagram of states to another. For example, in ST regime of starlike micelles ($M_B \geq M_B^*$),

$$\ln CMC \simeq -\left(\tau_B^2 N_B\right)^{2/3} + \left(\tau_B^2 N_B\right)^{2/5}\ln\left(\frac{H}{R}\right) \tag{70}$$

Branching of A block mediates the corona thickness H (eq 17), and affects CMC only *via* weak logarithmic term. However, an increase in n_B at a fixed length of backbone, M_B, (i.e., an increase in $N_B = M_B n_B$) leads to a rapid decrease in CMC compared to linear AB copolymer with DP M_B of insoluble block B.

For block copolymers with $M_B \leq M_B^*$, and number of superblobs $N_{BS} = aM_B/D_B \gg 1$, the first (dominant) term in eq 70 is unchanged while the sec-

ond term is modified according to the corresponding regime in the diagrams of states in Figures 6 and 7.

Notably, the values of scaling exponents for structural properties of spherical micelles in dilute solution differ from the scf exponents derived in ref.[20] The scaling model of starlike micelles developed in this paper imposes renormalization of bb block A into a flexible linear chain of impermeable superblobs with size D_A and effective Kuhn length $L_A \simeq D_A$, and implements the asymptotic $D_A(n_A)$ dependence for superblob thickness (i.e., as for cylindrical brush with $m_A \simeq 1$ and $n_A \gg 1$). In contrast, the scf model of starlike micelles[20] presumes almost unperturbed Gaussian size of the side chains in soluble block A, Gaussian elasticity of the backbone, and implements the mean-field approximation to account for binary monomer-monomer interactions. The latter is justified for semi-flexible corona chains (with ratio of Kuhn length to monomer size considerably larger than unity) in moderately good solvents.[49] In contrast to the scaling model, the distribution of the free ends of backbones is accounted *via* parabolic molecular potential originally introduced by Semenov.[50] As a result of different approximations, core radius R exhibits in the scf theory a weak power law dependence on N_A, $R \sim N_A^{-1/11} N_B^{7/11}$, while the scaling model predicts only logarithmic N_A-dependence, with $R \sim N_B^{3/5}$. Other exponents change correspondingly. However in spite of quite different approximations, the quantitative difference in predicted exponents is minor, and the trends in micelle behavior upon variations in architecture of the blocks are similar, so that both models can be used to confront the experimental data.

5.2 Comparison to experiments

In the presented scaling model the effective Kuhn length L is assumed to be on the order of superblob size in both bb blocks, $L_i \simeq D_i$ $(i = A, B)$, and sizes of all monomer units in the side chains and backbones are equal, $a_i = a$. Violation of the latter assumption would not affect the exponents in the power law dependences of micelle parameters while introduction of $L_i \gg D_i$ according to ref.[31] would invoke additional subregimes in the diagram of states. However due to relatively short side chains ($n_i < 10^2$) in the experimental systems discussed below, assumption $L_i \simeq D_i$ is reasonable.

Micellization of diblock copolymers with bb blocks was examined in a number of studies.[21–28] AB copolymers with water-soluble side chains in the corona block, e.g., PACMO,[24] PEO,[23] or PtBA[22] demonstrate the behavior inconsistent with the theoretical models. For instance, in contrast to the predicted increase in the core radius, $R \sim N_B^{\alpha}$, upon increasing N_B (with $\alpha = 3/5$ or $7/11$ in the scaling and scf models, respectively), micelles formed

by PACMO-PS block copolymer[24] with varied backbone length of the core-forming PS block ($15 \leq M_B \leq 75$, $n_B = 24$), did not exhibit distinct N_B-dependence, with values of R scattered around $\approx 25nm$. Also, SANS spectra did not allow for simple core-shell modelling, but were consistent with core-shell-shell structure of PACMO-PS micelles.

Starlike micelles formed by PEO-PLA[23] with core-forming PLA block of fixed N_B ($M_B = 75$, $n_B = 24$) and varied N_A of PEO block ($M_A = 75$, $8 < n_A < 56$) demonstrated non-monotonic dependence $R(N_A)$ in contrast to the theoretically predicted logarithmic decrease (scaling model), or weak power law dependence, $R \sim N_A^{-1/11}$ (scf model), upon increasing N_A. PEG-PCMA micelles[26] with fixed N_A of bb branched PEG block demonstrated strong non-monotonic dependence of hydrodynamic radius R_h on DP N_B of insoluble PCMA block, in contrast to the expected monotonic increase in $R_h \simeq R + H$ upon increasing N_B.

Elaborately tuned architectures of bb blocks in PEO-PLA micelles with end-functionalized PLA block[28] pointed at a critical role of the side chains in molecular packing and core loading capacity. All block copolymers had $N_A > N_B$, and formed spherical micelles with PEO coronas. However core-forming PLA blocks had relatively short backbones with side chains terminated with coumarin groups, and only one sample ($L_{2c}O - 57$) was characterized by cryo-TEM and DLS, to provide core radius $R = 15.5 \pm 2.5$ nm, corona thickness $H \approx 15$nm, and hydrodynamic radius $R_h = 117$ nm$/2 \approx 58$ nm. In $L_{2c}O - 57$ sample PLA block had 2 side chains per backbone monomer unit with $n_B = 15$ and $M_B = 29$. If the backbone of coumarin group is modelled as extra 3 PLA units, then $n_B \approx 15 + 3 = 18$. PEO block had $M_A = 38$, $n_A = 45$. Assuming close to theta-solvent conditions for PEO block ($\nu = 1/2$), and using eq 4, we estimate thickness $D_A/a \simeq n_A^{2/3} \approx 12.6$ for PEO block. Due to grafting of 2 side chains per one backbone monomer, thickness D_B of PLA block in $L_{2c}O - 57$ sample is estimated as $D_B/a \simeq (2n_B/\tau_B)^{1/2} \approx (18 \cdot 2/0.8)^{1/2} = 6.7$, with volume fraction of PLA monomer units $\tau_B \approx 0.8$ to account for own volume of coumarin groups. Therefore $D_A/D_B \approx 2$ for sample $L_{2c}O - 57$, as well as for all other samples ($L_{2c}O - 47, L_{2c}O - 43, L_{1c}O - 51, L_{1c}O - 45$) in the series with bb branched corona and core blocks. Positions of these samples are indicated in the scaling-type diagram of states constructed for $D_A/D_B = 2$ in **Figure 8**. As it is seen in figure 8, all the samples are close or above the dashed line in regime ST^2 at which the backbones in corona blocks approach maximal extension, $H \approx aM_A$, while the core radius R is specified by eq 40 with $\nu = 1/2$. For sample $L_{2c}O-57$ with PEO corona block ($a = 0.25$ nm), $H \approx 9.5$ nm, while radius of PLA core ($a = 0.375$ nm) is estimated as $R \approx 5.8$ nm. Note that

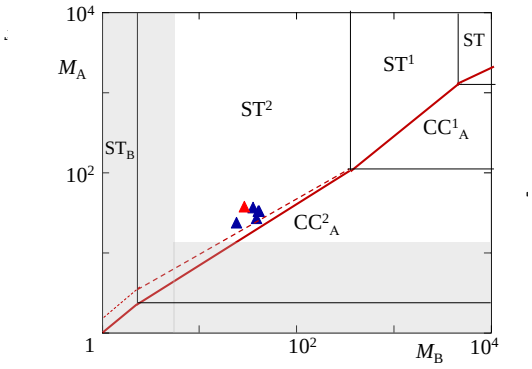

Figure 8: Location of experimental samples,[28] treated as block copolymers with asymmetrically branched bb blocks with $D_A/a = 12.6, D_B/a = 6.7, \tau_B = 0.8, \nu = 1/2$. All numerical prefactors are set equal to unity. Red symbol indicates sample L_2cO-57. Red line indicates boundaries between starlike and crew-cut micelles. At the dashed lines backbones of the corona blocks in starlike micelles approach maximal extension, $H = aM_A$. In shaded areas $aM_A \leq D_A$ or $aM_B \leq D_B$, corresponding to starlike shape of the corresponding block.

the theoretical estimates are done with the accuracy of numerical coefficients on the order of unity, and the difference in sizes of monomer units in side chains, and oxanorbornene backbone (with $a \approx 0.6$ nm) is neglected. In spite of these discrepances, the theoretical estimates fall in the proper range of experimental values, and the extended conformations of PLA and PEO backbones were detected in $L_{2c}O - 57$ micelles. At the same time, overall size of $L_{2c}O - 57$ micelles, $R + H \approx 30.5$nm (measured by cryo-TEM), was almost twice smaller than the hydrodynamic radius $R_h \approx 58$ nm (measured by DLS). Notably, according to the scaling model[45] R_h is expected to be smaller than $(R + H)$ by the size of last concentration blob in the corona of micelle.

A comprehensive study[21] focused on starlike spherical micelles formed by

di- and triblock copolymers with a variety of architectures in PS, PI and PB blocks in n-decane (soluble polydiene blocks) and dimethylacetamide (DMA) (soluble PS block). In PS-PI$^{\rm I}_x$ series, the number x of side chains in PI block varied from $x = 5$ to $x = 20$, and DP N_A of PI block was slightly (by $\simeq 10\%$) decreasing while DP N_B of PS block remained almost constant. An increase in x invoked weak monotonous increase in the core radius R from 6.5nm to 6.8nm, consistent with the predicted weak (logarithmic) dependence of R on DP N_A of the corona block A (eq. 18). Unfortunately, the data do not allow for a quantitative comparison with the theoretical dependences due to practically constant DPs of the blocks, and limited interval of solution concentrations.

Micelles formed in trifluoroethanol (TFE) by bb diblock copolymer with n-butylacrylate (nBuA) soluble block and carbazol-based bensyl acrylate (CzBA) insoluble block demonstrated[27] almost constant (within error bars) hydrodynamic radius R_h upon an increase in N_A and simultaneous decrease in N_B. These results are consistent with the scaling model of starlike micelle predicting that hydrodynamic radius, $R_h \simeq R + H$, with $R \sim aN_B^{3/5}$ and $H \sim aN_A^{3/5}N_B^{4/25}$ changes insignificantly upon variations in DPs of the blocks with $N_A + N_B \approx const$.

Recent study[25] provided a systematic data for the equilibrium parameters of spherical micelles in 1%wt solution of poly(5-perfluorooctyl norbornene-b-N-cyclohexyl-*exo*-norbornene-5,6-dicarboxyimide (PF-b-PC) block copolymer in THF (poor solvent for PF block). PF block contained densely grafted short side chains (C_8F_{17}) while DP M_B of this block, and DP N_A of linear PC block were varied. In scaling terms, short stiff side chains on norbornene backbone constitute oligomers with $n_B \simeq 1$. Therefore, one would expect that exponents in power law dependences for R and H might be close to the exponents for linear AB polymers.

In **Figure 9** radius R(nm) of micelle core[25] is presented as a function of DP M_B of the core-forming PF block for two molar masses of corona block A, 50kDa (red triangles) and 300kDa (blue squares), log-log coordinates. All symbols and error bars are the same as in the original study.[25] As it is seen in figure 9, an increase in $M_B = N_B/n_B$ leads to the monotonous increase in the core radius, R. According to the scaling model, $R \sim N_B^{3/5}$ depends on N_A only logarithmically, and slope 3/5 is indicated by a single line for both series (with 50kDa and 300kDa for block A). We also indicated slope 1 predicted for block copolymer with $N_B < N_B^*$ (regime ST$_B$). While slope 1 is plausible for series with smaller N_B (triangles), the exponent 3/5 fits the whole set of data better, and longer side chains and backbones are necessary to distinguish between the exponents.

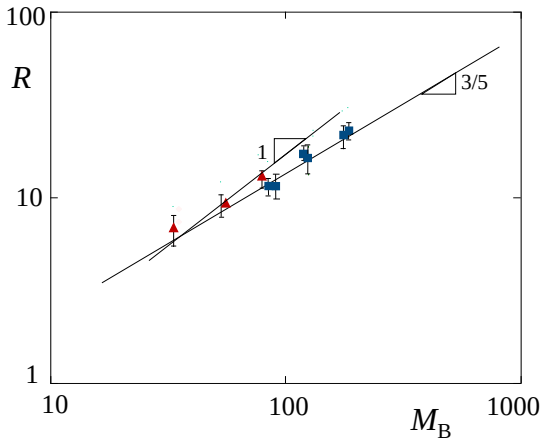

Figure 9: Radius of micellar core as a function of DP M_B of backbone in the core-forming PF block. Symbols and error bars are the same as in original study.[25] Solid lines have slopes 3/5 and 1, corresponding to conventional starlike and core-stretched micelles, respectively.

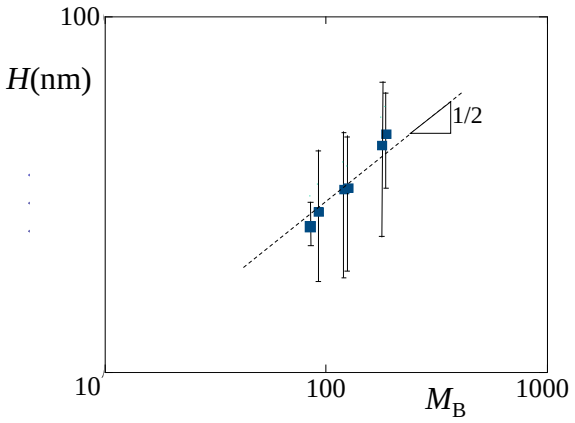

Figure 10: Corona thickness H (nm) as a function of DP M_B of backbone in core-forming PF block. Symbols and error bars are adopted from the original study.[25] Dashed line with slope 1/2, corresponds to core-stretched micelle with corona block under theta solvent conditions.

In **Figure 10** corona thickness H(nm) is presented as a function of M_B for series with 300kDa for block A. The value of exponent 0.74 estimated by the authors[25] was obtained in a too small interval of M_B variation to provide a reliable number. The slope 1/2 expected for theta-solvent conditions for block A ($\nu = 1/2$) in regime ST (shown by the dashed line in Figure 10) is also consistent with the experimental data, suggesting that the examined samples could be close to ST-ST$_B$ boundary. Clearly, more experiments with systematically varied lengths of flexible side chains and backbones are desirable to investigate the structure of spherical micelles with bb core and corona blocks to confront the theoretical models.

5.3 Conclusions

The scaling theory of micelles with bottlebrush (bb) corona- and core-forming blocks predicts a variety of regimes in a dilute solution. Compared to linear counterparts with DPs M_A and M_B of the blocks, the behavior of micelles is now additionally affected by thicknesses $D_A(n_A)$ and $D_B(n_B, \tau_B)$ of bb blocks. Bb branching of soluble block A induces power law dependence on n_A in the equilibrium parameters of micelles. In contrast, bb branching of long insoluble block B does not induce power law dependence on n_B in the micelle parameters but affects CMC and coil-to-globule transition of block B. The effect of n_B manifests itself at DP $M_B \leq M_B^*$ of the backbone in core block. In this range of molecular parameters, backbones in the core (regime ST$_B$) or corona (regimes CC^1, CC^2), or in both, core and corona (regime CC$_{A,B}$) blocks approach full stretching, giving rise to micelles that exhibit novel power law dependences in Q, R, and H. Notably, the numerical estimates of M_B^* below which micelles could have strongly extended backbones, indicate that many experimental systems with bb block copolymers fall in the range of $M_B < M_B^*$, and therefore the data rationalization could require the scaling model developed in this paper.

Associated Content

Supporting Information: Scaling theory of collapse of bottlebrush macromolecule in poor solvent

Acknowledgment

This work was supported by Russian Science Foundation, grant 20-13-00270

References

[1] Kataoka, K.; Haradaa, A.; Nagasaki, Y. Block copolymer micelles for drug delivery: design, characterization and biological significance. *Advanced Drug Delivery Reviews* **2001**, 47 (1), 113-131.

[2] Ibrahimova, V.; Zhao, H.; Ibarboure, E. ; Garanger, E.; Lecommandoux, S. Thermosensitive vesicles from chemically encoded lipid-grafted elastin-like polypeptides. *Angewandte Chemie* **2021**, DOI: 1002/ange.303102807.

[3] Vatankhah-Varnosfaderani, M.; Keith,A. N.; Cong, Y.; Liang, H.; Rosenthal, M.; Sztucki, M. ; Clair, C. ; Magonov, S.; Ivanov, D.A. ; Dobrynin, A.V.; Sheiko, S.S. Chameleon-like elastomers with molecularly encoded strain-adaptive stiffening and coloration. *Science* **2018**, *359 (6383)*, 1509-1513.

[4] Gohy, J.-F. Block Copolymer Micelles. *Adv. Polym. Sci.* **2005**, *190(1)*, 65-136.

[5] Lazzari, M.; Lin, G.; Lecommandoux, S. *Block copolymers in nanoscience*; Wiley-VCH: Weinheim 2006

[6] Li, Z.; Tang, M.; Liang, S.; Zhang, ; Biesold, ; He, Y.; Hao, ; Choi, W.; Liu, Y. ; Peng, J.; Lin, Z. Bottlebrush polymers: From controlled synthesis, self-assembly, properies to applications. *Progress in Polymer Science* **2021**, *116*, 101397.

[7] Borisov, O.V.; Zhulina, E.B.; Leermakers, F.A.M.; Müller, A.H.E. Self-Assembled Structures of Amphiphilic Ionic Block Copolymers: Theory, Self-Consistent Field Modeling and Experiment. *Adv. Polym. Sci.* **2011**, *241*, 57-130.

[8] de Gennes, P.-G. *Scaling Concepts in Polymer Physics*. Cornell University Press: Ithaca and London, 1979

[9] Alexander, S. Adsorption of chain molecules with a polar head: a scaling description. *J.Phys.(France)*, **1977**, *38*, 983-987

[10] de Gennes P.-G. Conformations of Polymers Attached to an Interface. *Macromolecules*, **1980**, *13*, 1069-1075

[11] De Gennes, P.-G. Macromolecules and Liquid Crystals: Reflections on Certain Lines of Research. *Solid State Phys., Suppl.***1978**, *14*, 1-18.

[12] Zhulina, Ye. B.; Birshtein, T.M. Conformations of Block Copolymer Molecules in Selective Solvents. (Micellar Structures). *Polymer Science USSR* **1985**, *27*, 570-578;

[13] Birshtein, T.M.; Zhulina, E.B. Scaling Theory of Supermolecular Structures in Block Copolymer - Solvent Systems. 1. Model of Micellar Structures. *Polymer* **1989**, *30 (1)*, 170 - 177.

[14] Halperin, A. Polymeric micelles: a star model. *Macromolecules* **1987**, *20 (11)*, 2943–2946.

[15] Volkova, L.A., Andreeva, N.A., Podolosky, A.F., Bitsenko, M.I., Eskin, V.A. Study of mesomorphic properties of solutions of triblock copolymer: polyisoprene-poly-α-methyl styrene-polyisoprene. *Vysokomol. soedin. A* **1982**, *24*, 1180-1185

[16] Shibayama, M., Hashimoto, T., Kawai, H. Ordered structure in block polymer solutions. 1. Selective solvents. *Macromolecules* **1983**, *16*, 16-28.

[17] Molina, J.J.; Pierleoni, C.; Capone, B.; Hansen, J.-P.; Santos de Oliveira, I.S. Crystal stability of Diblock Copolymer Micelles in Solution. Molecular Physics **2009**, *107*, 535-548.

[18] Marras, A.E.; Campagna, T.R.; Vieregg, J.R.; Tirrell, M.V. Physical Property Scaling Relationships for Polyelectrolyte Complex Micelles. *Macromolecules* **2021**, DOI: 10.1021/acs.macromol.1c00743.

[19] Semenov, A. N.; Joanny, J.-F.; Khokhlov, A. R. Associating polymers: Equilibrium and linear viscoelasticity. *Macromolecules* **1995**, *28 (4)*, 1066–1075.

[20] Lebedeva, I.O.; Zhulina, E.B.; Borisov, O.V. Self-assembly of bottlebrush block copolymers in selective solvent: micellar structures. *Polymers* **2021**, *13*, 1351-1365.

[21] Zamurovic, M.; Christodoulou, S.; Vazaios, A.; Iatrou,E.; Pitsikalis, M.; Hadjichristidis, N. Micellization Behavior of Complex Comblike Block Copolymer Architectures. *Macromolecules* **2007**, *40*, 5835-5849.

[22] Li, Z.; Ma, J.; Xheng, C.; Zhang, K.; Wooley, K.L. Synthesis of Hetero-Grafted Amphiphilic Diblock Molecular Brushes and Their Self-Assembly in Aqueous Medium. *Macromolecules* **2010**, *43*, 1182-1184.

[23] Fenyves, R.; Schmutz, M.; Horner, I.J.; Bright, F.V.; Rzaev, J. Aqueous Self-Assembly of Giant Bottlebrush Block Copolymer Sufactants as Shape-Tunable Building Blocks. *J.Am.Chem.Soc.* **2014**, *136*, 7762-7770.

[24] Alaboalirat, M.; Qi, L.; Arrington, K.J.; Qian, S.; Keum, J.K.; Mei, H.; Littrell, K.C.; Sumpter, B.G.; Carrillo, J.-M. Y.; Verduzco, R.; Matson, J.B. Amphiphilic Bottlebrush Block copolymers: Analysis of Aqueous Self-Assembly by Small-Angle Neutron Scattering and Surface Tension Measurements. *Macromolecules* **2019**, *52(2)*, 465–476.

[25] Kim, S.; Cho, Y.; Kim, J.H.; Song, S.; Lim, J.; Choi, S.-H.; Char, K. Structural Analysis of Bottlebrush Block Copolymer Micelles Using Small-angle X-ray Scattering. *ACS Macro Lett.* **2020**, *9*, 1261-1266.

[26] Taipaleenmaki, E.; Mouritzen, S. A.; Schattling, P. ; Zhang, Y.; Städler, B. Mucopenetrating micelles with a PEG corona. *Nanoscale* **2017**, *9 (46)* , 18438-18448.

[27] Wang, Y.; Shao, F. ; Sauve, E.R.; Tonge, C.M.; Hudson, Z.M. Self-assembly of giant bottlebrush block copolymer surfactants from luminescent organic electronic materials. *Soft Matter* **2019**, *15*, 5421-5430.

[28] Unsal, H. ; Onbulak, S. ; Calik, F. ; Er-Rafik, M.; Schmutz,M.; Sanyal,A.; Rzayev, J. Interplay between Molecular Packing, Drug Loading, and Core Cross-Linking in Bottlebrush Copolymer Micelles. *Macromolecules* **2017**, *50(4)*, 1342–1352.

[29] Paturej, J.; Sheiko, S. S.; Panyukov, S. ; Rubinstein, M. Molecular structure of bottlebrush polymers in melts. *Sci. Adv.* **2016**, *2*, e1601478.

[30] Birshtein, T. M.; Borisov, O. V.; Zhulina, Y. B. ; Khokhlov, A. R.; Yurasova, T. A. Conformations of comb-like macromolecules. *Polym. Sci. U.S.S.R.* **1987**, *29*, 1293–1300.

[31] Fredrickson, G. H. Surfactant-induced lyotropic behavior of flexible polymer solutions. *Macromolecules* **1993**, *26*, 2825–2831.

[32] Subbotin, A. V.; Semenov, A. N. Spatial Self-Organization of Comb Macromolecules. *Polym. Sci., Ser. A* **2007**, *49*, 1328-1357.

[33] Saariaho, M.; Ikkala, O. ; Szleifer, I. ; Erukhimovich, I. ; ten Brinke, G. On lyotropic behavior of molecular bottle-brushes: A Monte Carlo computer simulation study. *J. Chem. Phys.* **1997**, *107*, 3267–3276.

[34] Saariaho, M.; Szleifer, I. ; Ikkala, O. ; ten Brinke, G. Extended conformations of isolated molecular bottle-brushes: Influence of side-chain topology. *Macromol. Theor. Simul.* **1998**, *7*, 211–216.

[35] Subbotin, A. ; Saariaho, M.; Ikkala, O.; ten Brinke, G. Elasticity of comb copolymer cylindrical brushes. *Macromolecules* **2000**, *33*, 3447–3452.

[36] Elli, S. ; Ganazzoli, F.; Timoshenko, E. G.; Kuznetsov, Y. A.; Connolly, R. Size and persistence length of molecular bottle-brushes by Monte Carlo simulations. *J. Chem. Phys.* **2004**, *120*, 6257–6267.

[37] Feuz, L.; Leermakers, F. A. M.; Textor, M.; Borisov, O. Bending rigidity and induced persistence length of molecular bottle brushes: A self-consistent-field theory. *Macromolecules* **2005**, *38*, 8891–8901.

[38] Rathgeber, S.; Pakula, T.; Wilk, A.; Matyjaszewski, K.; Beers, K.L. On the shape of bottle-brush macromolecules: systematic variation of architectural parameters.*J. Chem. Phys.* **2005**, *122(12)*, 124904.

[39] Hsu, H.-P.; Paul, W. ; Binder, K. Standard definitions of persistence length do not describe the local intrinsic stiffness of real polymer chains. *Macromolecules***2010**, *43*, 3094–3102.

[40] Hsu, H.-P. ; Paul, W. ; Binder, K. Estimation of persistence lengths of semiflexible polymers: Insight from simulations. *Polym. Sci. Ser. C* **2013**,*55*, 39–59.

[41] Theodorakis, P. E.; Hsu, H.-P.; Paul, W.; Binder, K. Computer simulation of bottle-brush polymers with flexible backbone: Good solvent versus theta-solvent conditions.*J. Chem. Phys.* **2011** *135*, 164903.

[42] Borisov, O.V.; Zhulina, Y.B.; Birshtein, T.M. Diagram of the State and Collapse of Grafted Chain Layers. *Polymer Science USSR* **1988**, *30*, 772-779.

[43] Polotsky, A.; Daoud, M.; Borisov, O. Analysis of the Longitudianl Structure of a Collapsed Molecular Bottle Brush Using a Self-Consistent Field Approach. *Int. J. Polymer Anal. Char.* **2007**, *12*, 47-55.

[44] Daoud, M.; Cotton, J.-P. Star shaped polymers : a model for the conformation and its concentration dependence. *Journal de Physique (France)* **1982**, *43 (3)*, 531-538.

[45] Zhulina, E.B.; Adam, M. ; Sheiko, S. ; LaRue, I. ; Rubinstein, M. Diblock Copolymer Micelles in a Dilute Solution. *Macromolecules* **2005**, *38*, 5330 - 5351.

[46] Zhulina, E.B.; Sheiko, S.S.; Dobrynin, A.V.; Borisov, O.V. Microphase segregation in the melts of bottlebrush block copolymers. *Macromolecules* **2020**, *53 (7)*, 2582-2593.

[47] LaRue, I.; Adam, M.; Zhulina, E.B.; Rubinstein,M.; Pitsikalis, M.; Hadjichristidis, N.; Ivanov, D.A.; Gearba, R.I.; Anokhin, D.V.; Sheiko, S.S. Effect of the Soluble Block Size on Spherical Diblock Copolymer Micelles. *Macromolecules* **2008**, *41 (17)*, 6556-6563.

[48] Hassouneh, W.; Zhulina, E. ; Chilkoti A.; Rubinstein, M. Elastin-like Polypeptide Diblock Copolymers Self-assemble into Weak Micelles - *Macromolecules* **2015**, *48 (12)*, 4183–4195.

[49] Birshtein, T.M.; Zhulina, E.B. Conformations of Star-Branched Macromolecules. *Polymer* **1984**, *25 (10)*, 1453 - 1461.

[50] Semenov, A. N. Contribution to the theory of microphase layering in block copolymer melts. *Sov. Phys. JETP.* **1985**, *61*, 733-742.